Ecosystems (2023) 26: 687–705
https://doi.org/10.1007/s10021-022-00786-1

Topography Mediates the Response of Soil CO_2 Efflux to Precipitation Over Days, Seasons, and Years

Marissa Kopp,[1]* Jason Kaye,[1] Yuting He Smeglin,[2] Thomas Adams,[3] Edward J. Primka IV,[1,4] Brosi Bradley,[1] Yuning Shi,[3] and David Eissenstat[1]

[1]*Department of Ecosystem Science and Management, Pennsylvania State University, 116 ASI Building, University Park, Pennsylvania 16802, USA;* [2]*Department of Meteorology and Atmospheric Science, Pennsylvania State University, University Park, Pennsylvania, USA;* [3]*Department of Plant Science, Pennsylvania State University, University Park, Pennsylvania, USA;* [4]*Department of Natural Resource Ecology and Management, Oklahoma State University, Stillwater, Oklahoma 74078, USA*

Abstract

Spatiotemporal heterogeneity in soil CO_2 efflux (F_S) underlies one of our greatest gaps in understanding global carbon (C) cycles. Though scientists recognize this heterogeneity, F_S sampling schemes often average across spatial heterogeneity or fail to capture fine temporal heterogeneity, and many ecosystem models assume flat terrain. Here, we test the idea that simple, remotely sensible terrain variables improve regression models of spatiotemporal variation in F_S. We used automatic chambers that, for the first time, capture F_S in complex temperate forest terrain at fine temporal resolution with 177,477 hourly F_S measurements at 8 locations from ridgetop to valley along planar and swale hillslopes, across three years ranging from dry to record wet precipitation. In two of these years, we measured F_S weekly at 50 additional locations distributed across the 8-ha catchment. Growing season Fs estimates were 1.25 times greater when sampling hourly versus weekly. At ridgetops, growing season F_S increased by an average of 463 gC m^{-2} 180 day^{-1} (75.9%) from dry to wet years, while valleys decreased by 208 gC m^{-2} 180 day^{-1} (− 20.1%). This bidirectional response to interannual moisture was identified in distinct Random Forest models of Fs for convergent (water accumulating) or non-convergent (water shedding) hillslope positions. We hypothesize that different F_S constraints drive these opposing responses—water availably to biota limits F_S from ridgetops while slow oxygen diffusion limits F_S from wet valleys. Accounting for hillslope position and shape reduces variance of F_S estimates in complex terrain, which could improve F_S sampling, C budgets, and modeling.

Key words: topography; soil CO_2 efflux; soil respiration; climate variability; critical zone; complex terrain.

Highlights

- Simple terrain metrics of hillslope position and shape reduce variance in F_S estimates
- Ridgetop F_S was highest in a wet year, while valley floor F_S was highest in a drought

Received 6 May 2022; accepted 13 August 2022;
published online 15 September 2022

Supplementary Information: The online version contains supplementary material available at https://doi.org/10.1007/s10021-022-00786-1.

Author Contributions: Secured funding: DE, JK, Conceptualized and designed study: JK, DE, TA, Collected data and maintained the experiment: TA, BB, EP, Modeled soil moisture and temperature data: YHS, YS, Conducted statistical analyses: MK, Prepared the first manuscript draft/led writing: MK, JK, Revised manuscript: All.

**Corresponding author; e-mail:* mkk5565@psu.edu

- Growing season F_S estimated from hourly sampling was about 1.25x greater than from weekly sampling

Introduction

Soil CO_2 efflux (F_S), the release of CO_2 from soils to the atmosphere, is the second largest flux in the global carbon (C) cycle (Friedlingstein and others 2020). An estimated 90 Pg CO_2-C diffuse from soils to the atmosphere each year, roughly 10 times larger than annual global anthropogenic CO_2 emissions (Schlesinger and others 2013), and potentially increasing at a rate of about 0.1 Pg C year^{-1} (Bond-Lamberty and Thomson 2010; Hashimoto and others 2015). Despite its importance, the land surface exchange of CO_2 with terrestrial ecosystems bears the largest uncertainty bounds in current global C budgets (Todd-Brown and others 2013; Friedlingstein and others 2014). In fact, F_S is often estimated as a residual from other, better-known variables in the global C budget (for example, Le Quéré and others 2016).

Spatial heterogeneity contributes to the uncertainty in F_S. Although F_S has been measured extensively in the past century (Jian and others 2021), these point measurements are scaled to ecosystem, landscape, or global estimates using modeling frameworks that assume flat terrain (for example, Dai and others 2004; Mao and others 2016): an assumption violated by over 50% of the global land surface (Rotach and others 2014). Areas of complex terrain can be significant terrestrial sinks of atmospheric CO_2; for example, Reyes and others (2017) estimate about 15% of C sequestration in the conterminous US occurs in topographically complex areas. Complex terrain influences soil temperature, as well as the lateral distribution of water, sediments, nutrients, and C, all of which may influence F_S. Research from the Susquehanna Shale Hills Critical Zone Observatory (CZO) (where our field site is located) revealed significant relationships between topography and soil organic C storage (Andrews and others 2011), soil pCO_2 (Hasenmueller and others 2015; Hodges and others 2019), and aboveground and belowground tree C storage (Smith and others 2017; Orr 2016). This complements a growing body of evidence linking topography to the spatial distribution of C fluxes (for example, Pacific and others 2011; Shi and others 2018; Smeglin and others 2020) and the response of these fluxes to climatic changes (for example, Riveros-Iregui and McGlynn 2009; Berryman and others 2015; Reyes and others 2017).

Despite the significance of topography as a mediator of C cycling, explicit study of F_S in complex terrain remains limited. The only thorough case studies we are aware of were in the US Rocky Mountain range (for example, Pacific and others 2008; Riveros-Iregui and McGlynn 2009; Riveros-Iregui and others 2012; Berryman and others 2015). At these sites, lateral redistribution of soil water from non-convergent (water shedding) to convergent (water accumulating) areas led to bidirectional responses of F_S to interannual precipitation variability: landscape positions receiving high drainage had higher cumulative F_S in a drought year, whereas positions with low drainage had higher Fs in a non-drought year (Riveros and others 2012). Although such work has provided a nascent understanding of mechanisms underpinning F_S variability across climate and topography, the pervasiveness of complex terrain on the global land surface calls for expanded exploration beyond these (sub)alpine ecosystems (Reyes and others 2017). For example, the idea that soil saturation decreases F_S is well established in laboratory incubations and wetlands (for example, Doran and others 1991). Yet very few field studies identify which upland areas may be impacted by this process and to what extent. Additionally, many Earth System Models do not capture the lateral redistribution of water that drives these patterns (Clark and others 2015).

New understanding of F_S in complex terrain may be advanced by higher temporal resolution data. The spatial distribution of soil moisture can change rapidly in complex terrain as preferential flow paths redistribute rainwater. For example, at the Shale Hills CZO, preferential soil water flow paths cause high moisture following rain events to be fleeting on ridgetops and planar slopes as water is drained to convergent landscape positions in swales and the valley floors (Lin and others 2006). These rainfall events rapidly alter soil pCO_2 at Shale Hills (for example, Hodges and others 2019) and Fs in other forests in complex terrain (for example, Riveros-Iregui and others 2008). Thus, rainfall events can change F_S within sub-weekly timescales, with the magnitude and lag time of response related to topographic positions (Petrakis and others 2017; Riveros-Iregui and others 2008). Yet, with so few high temporal resolution Fs measurements, we lack a generalized understanding of how topography mediates the Fs response to moisture change. It is possible that a unit change in soil moisture produces the same change in Fs at a ridgetop and a valley floor, but this assumption has rarely been tested, and it may be wrong for soils that remain saturated. For example, extended anaerobic conditions in convergent areas may lead to lower *F*s at a given soil moisture than nonconvergent areas with brief saturation.

There are inherent tradeoffs between temporal and spatial resolution when designing sampling schemes of F_S in complex terrain (Lovett and others 2005). Explorations of F_S across topographic gradients often use manual chambers, allowing for many replicates across space (for example, Riveros-Iregui and others 2012; Savage and Davidson 2001). However, collecting and processing samples from manual methods is labor intensive, which leads to sampling frequencies rarely finer than weekly (Riveros-Iregui and McGlynn 2009; Riveros-Iregui and others 2012) and, more often, as low as fortnightly (Berryman and others 2015) or monthly (Hanson and others 1993; Wang and others 2019; Jiang and others 2020). Further, manual sample collection typically excludes nighttime fluxes (for example, Hanson and others 1993; Riveros-Iregui and McGlynn 2009; Riveros-Iregui and others 2012; Berryman and others 2015; Wang and others 2019; Jiang and others 2020). Thus, while manual methods may capture spatial heterogeneity in F_S at longer timescales (Savage and Davidson 2003), they miss the fine temporal responses.

By contrast, automatic chambers enable continuous F_S observations at hourly or sub-hourly temporal resolutions that capture nighttime fluxes and short-term responses to rain (Savage and Davidson 2003; Ruehr and others 2009; Görres and others 2016). While automatic chambers have been increasingly used to measure F_S, many of these studies do not explicitly consider topographic variation (Makita and others 2018; Courtois and others 2019). Studies that do consider topography have often been limited in execution, such as one automatic chamber (Ruehr and others 2010) or one year of measurement (Liu and others 2006; Ruehr and others 2010; Tian and others 2019), with notable exceptions focused on tropical forests or plantations (Rubio and Detto 2017; Yan and others 2019). Overall, automatic chambers remain an underutilized tool in identifying the timing of spatial controls on ecosystem-level F_S that may be necessary for scaling F_S responses to global change.

In this study, we present one of the first multiyear, continuous datasets of F_S in a temperate deciduous forest in complex terrain. Within this dataset, we analyze F_S across three years representing a gradient from drought to record precipitation. We use these data to ask: how does topography influence the response of F_S to interannual precipitation variability? We hypothesize that (1) adding terrain variables to standard soil temperature and moisture predictors will explain significantly more variance in estimates of growing season and daily F_S across climate variability, and (2) automated chamber methods will provide the same F_S estimates as manual sampling when aggregated to the growing season temporal scale and catchment spatial scale.

Methods

Site Description

We designed our soil CO_2 efflux (F_S) sampling scheme to capture topographic variability (Figure 1) in the Shale Hills watershed (40°40′N, 77°54′W) of the Susquehanna Shale Hills Critical Zone Observatory (He 2019). The Shale Hills watershed is a small (0.08 km^2), forested, first-order catchment underlain by Rosehill shale bedrock. Catchment topography includes steep planar slopes alternating with areas of convergent flow, known as swales (Brantley and others 2018). This convergence influences productivity in the mature oak-dominated (*Quercus* sp.) deciduous broadleaf forest, with evidence of greater aboveground carbon uptake and storage in swales and valley floors compared to ridgetops and planar slopes (Smith and others 2017). Hillslope curvature and position also drive soil carbon, texture, and depth, with valley floor positions having deeper and wetter soils with a greater clay content than the ridgetop soils (Lin and others 2006; Supplemental Table 1). We sampled across convergent (swale) and nonconvergent (planar) slopes, as well as positions along these hillslopes (ridgetop, midslope, and valley floor, by elevation). Though the landscape can also be considered a continuous variable (for example, Riveros-Iregui and McGlynn 2009), we use these categories as one approach to define replicates, discuss trends across topography, and propose a method for upscaling F_S in global models. Overall, this sampling design enables us to analyze F_S within nested scales: at the level of chambers, of landscape positions, and by the presence or absence of convergent flow.

Shale Hills has a humid continental climate with a mean annual temperature of 10 °C and mean annual precipitation of 1050 mm (NOAA 2007). However, annual precipitation from 2016 to 2018 deviated from this average: 2016 was a drought year at 719 mm, 2017 was near average at 988 mm, and 2018 was a wet year at 1275 mm (Xiao and Li 2018). Put in a state historical context,

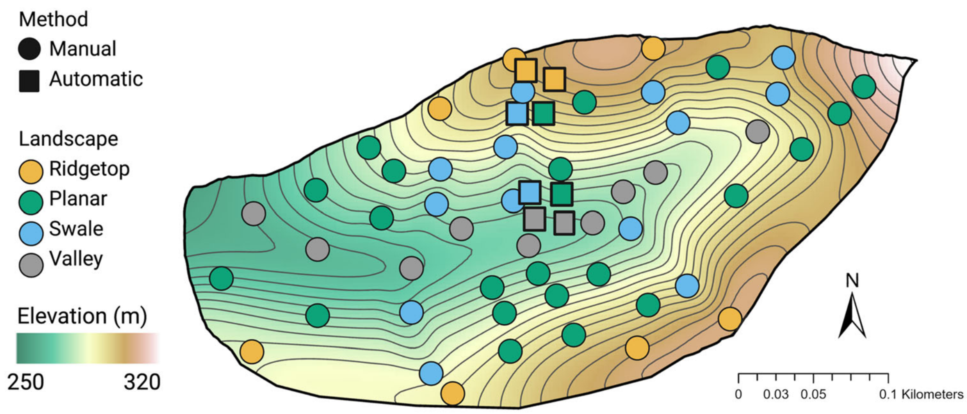

Figure 1. Location of soil CO_2 efflux (F_S) measurements along elevation map of Shale Hills with 2-m topographical contoured lines. F_S was measured at four landscape positions: ridgetops (yellow), planar midslopes (green), swales (blue), and valley floors (gray). Measurements were collected using both automatic chambers (where squares represent the soil collar) and manual methods (where circles represent the 10-m-diameter circular macroplots, within which were three soil collars averaged to the macroplot scale).

2016 was the second driest year in Pennsylvania in the last two decades and 2018 was the wettest year on record (NOAA 2021). We targeted our analyses across these three years to explore the response of F_S to rapid and significant change in interannual water availability.

Automatic Soil CO_2 Efflux Collection

F_S was measured hourly in two replicates across four landscape positions (ridgetop, planar midslope, swale midslope, and valley floor) using an automated soil respiration instrument, the LI-8100A Soil CO_2 Flux System (LI-COR Biosciences Inc., Lincoln, NE, USA). Two LI-8100A Flux Systems were each linked to four opaque long-term soil respiration chambers (8100-104) fitted to a LI-8150 Multiplexer. These chambers measure F_S by closing over a soil collar installed to $\sim$ 5 cm depth and continuously calculating the change in CO_2 concentrations within the chamber over 120 s, allowing 20 s for chamber closure, 30 s as a ''dead band'' to reach steady mixing immediately after closure, and 30 s after measurement for air to purge sampling lines of moisture. After completing the measurement, the chamber moves 180° from the soil collar to preserve the natural CO_2 gradient between soils and the atmosphere. Data were downloaded approximately weekly, at which time we removed any plant growth within the chambers and debris that could affect the chamber's closure. Otherwise, all new litter inputs were allowed to accumulate in the collars. Measurements were stopped prior to forecasted snowfall to avoid damaging the automated systems. Samples were taken every hour from July 2015 to December 2018 which, when accounting for missing data from technical issues and inclement weather, led to a total of 177,477 observations. This base dataset is publicly available through COSORE (Bond-Lamberty and others 2020).

F_S was estimated using SoilFluxPro software (version 4, LI-COR Biosciences). F_S was calculated as both an exponential and linear regression of CO_2 concentration in the chamber over time. The best-fitting model was determined by comparing the regression coefficient (R^2) and the normalized sums of the squares of the residuals for both fits. All calculations discarded the first 30 s of the CO_2 concentration curves to account for disturbances of soil surface pressure from the chamber movement (Courtois and others 2019).

F_S estimates from the base dataset were removed using the following quality control pipeline: (1) incomplete entries (n = 1506); (2) fluxes that had a best-fitting regression between time and CO_2 concentration with an $R^2 < 0.90$ (n = 13,394) as per literature precedent (Courtois and others 2019; Savage and others 2014); (3) entries with known problematic data according to the field technician error log (n = 1264); and (4) entries with physically implausible values (fluxes < -1 or > 50 µmol m^{-2} s^{-1}) (n = 34). Additionally, fluxes that were ± 5 µmol m^{-2} s^{-1} from adjacent observations were flagged as ''spikes'' (Rubio and Detto 2017). The regression between time and CO_2 concentration for each ''spike'' was individually reviewed and removed if there was evidence of measurement errors (n = 479), such as implausibly high starting CO_2 concentrations (suggesting that not enough time elapsed between chamber closings to preserve the CO_2 concentration gradient) or erratic concentrations (suggesting an improper seal between the chamber and soil collar). After following these criteria, 90.6% of original flux measurements were retained (Figure 2).

Manual Soil CO_2 Efflux Collection

F_S was manually measured weekly to biweekly in 2016–2017 between 0900 and 1400 h because prior research suggested this time window may minimize diel effects (Davidson and others 1998). Measurements were collected at 50 macroplot sites (Figure 1) spanning ridgetops ($n = 7$), planar midslopes ($n = 21$), swale midslopes ($n = 13$), and valley floors ($n = 9$). Within these 10-m diameter circular macroplots, F_S was measured at three soil collars with the same LI-COR 8100 analyzer used for continuous observations. At each sampling time, soil collar F_S was averaged to the macroplot scale to account for spatial autocorrelation. Spatial measurements were checked for quality, such that values indicating a malfunction (that is, unreasonable chamber temperature, initial CO_2, or pressure, etc.) were removed. We calculated growing season estimates as a linear interpolation between daily observations (for example, Pacific and others 2008), which were summed for the 180 days between May 9 to October 15 (the earliest and latest sampling dates found in both years).

Co-located Timeseries and Geospatial Data

To understand controls on F_S, we leveraged co-located time series data available from the Shale Hills CZO (https://czo-archive.criticalzone.org/shale-hills/data/datasets/). For climate variables, this included hourly precipitation from an OTT Pluvio weighing rain gauge gap-filled with data from the National Atmospheric Deposition Program (Xiao and Li 2018). Hourly air temperature was measured in the automated chambers and gap-filled with regional Daymet climate data (Thornton and others 2020) adjusted for our study site using the R ''daymetr'' package (version 1.6) (Hufkens and others 2018). For metrics of plant productivity, an indicator of autotrophic respiration, we used 90th percentile daily green chromatic coordinate (GCC), an estimate of canopy greenness from PhenoCam imagery (Richardson and others 2018). For biophysical controls on heterotrophic respiration, we monitored soil moisture using ECH2O EC-5 or GS1 (Decagon, METER Group Inc, Pullman, WA, USA) sensors and soil temperature using 8150-203 soil temperature probes (LI-COR) at 5-cm soil depth co-located with each chamber. However, the sensors often failed or recorded physically impossible data.

Instead, we modeled hourly soil moisture and temperature at a 5-cm depth using the Penn State Integrated Hydrologic Model with a surface heat flux module (Flux-PIHM; Shi and others 2013). Flux-PIHM is a physically based, spatially distributed, land surface hydrologic model that simulates lateral water flows (Shi and others 2013), which are critical to capturing heterogenous F_S in complex topography (Riveros-Iregui and others 2012). In the Shale Hills watershed, Shi and others (2015) have found that Flux-PIHM simulates the dynamic and spatial structure of observed soil moisture. Specifically, the Shale Hills watershed model domain was decomposed into a triangular network of 532 grids. Flux-PIHM simulations used a surface elevation map from lidar measurements (Guo 2019), a soil map and soil hydraulic properties from an extensive soil survey (Lin and others 2006), and a vegetation map from a survey of more than 2000 trees (Eissenstat and others 2013). The meteorological forcing data for Phase 2 of the North American Land Data Assimilation system (NLDAS-2; Xia and others 2012) were used for the model simulation. The model was calibrated using discharge, groundwater level, soil moisture, soil temperature, and surface heat flux measurements. Model-predicted spatial patterns of soil moisture at a 5-cm depth have been validated using field measurements (Shi and others 2015), which showed that the model is able to capture the observed macro-spatial pattern of soil moisture at Shale Hills. We used the modeled soil temperature and soil moisture as liquid water of the topsoil layer (0–10 cm) at the corresponding grids where automated chambers were located. Note that soil moisture, here, is the volume of liquid water, which excludes the frozen soil moisture content.

Additionally, we gathered static (or slow changing) variables using soil samples and remote sensing products (Supplemental Table 1). In June 2020, we collected two soil cores within 1 m of each chamber to a 15-cm depth using a 5.08-cm-diameter split corer. Each soil core was split into two layers for uniform processing: ''surface'' mineral soils from 0 to 5 cm, and ''deeper'' mineral soils from 5 to 15 cm. We collected O horizons within a 24-cm ring centered around each core. Samples were placed on ice and transported back to the laboratory where they remained at 4 °C until processing. Soils were dried to constant mass to determine water content gravimetrically. Soil bulk

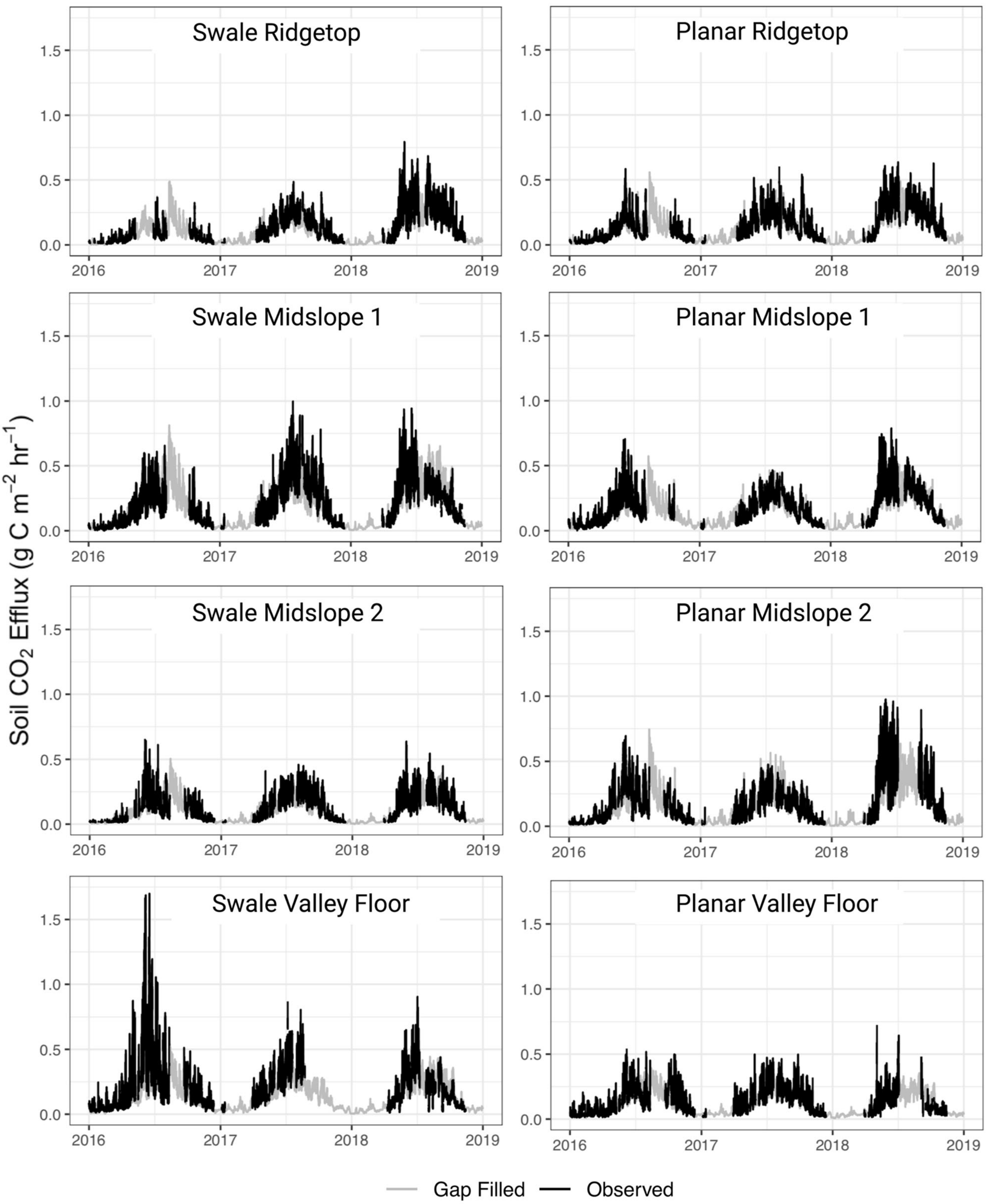

Figure 2. Time series of soil CO_2 efflux across three years of measurement. Black lines indicate quality controlled observations, while gray lines represent gap-filling through a regression model with modeled 5-cm soil temperature and volumetric soil water content (see Eq. 2). Year tick marks correspond to January 1.

Table 1. Growing Season F_S Mean ± Standard Error (g C m^{-2} 180 day^{-1}) by Landscape Position and Sampling Method

	Growing season F_S (g C m^{-2} 180 $days^{-1}$)				
	2016		2017		2018
	Automatic	Manual	Automatic	Manual	Automatic
Ridgetop	610 ± 63	513 ± 29	748 ± 34	719 ± 44	1073 ± 8
Planar midslope	926 ± 17	598 ± 36	838 ± 2	761 ± 50	1350 ± 139
Swale midslope	908 ± 204	655 ± 40	1068 ± 291	846 ± 60	1070 ± 295
Valley	1036 ± 240	664 ± 36	876 ± 109	880 ± 54	828 ± 113
Annual precipitation (mm)	719		988		1275

Growing season F_S from automatic chambers (n = 2 chambers per landscape position) was calculated as the sum of all gap-filled hourly observations for the 180 days between May 9 and Oct 15 of each year. Growing season F_S from manual sampling (n = 7 to 21 chambers per landscape position) was estimated as a linear interpolation between daily observations (for example, Pacific and others 2008), which were summed between May 9 to Oct 15. Manual data were not collected in 2018.

density was calculated both with and without rock volume (Throop and others 2012). O horizon samples were ground to 1 mm using a Wiley Mill, and mineral soils were sieved at 2 mm. Soil texture was determined using the rapid method from Kettler and others (2001). Soils were analyzed for total C at Penn State Agricultural Analytical Laboratories using the combustion method (Nelson and Sommers 1996).

We estimated topographic variables in ArcGIS Pro using a 3-m Digital Elevation Model (Guo 2019). Soil depth was calculated as elevation minus bedrock elevation, determined from ground penetrating radar (Lin 2019). Three types of curvature were calculated using the Curvature function: profile, or curvature parallel to the slope, which relates to rates of erosion and deposition; planform, or curvature perpendicular to the slope, which relates to flow convergence; and standard, which combines both types of curvature into a standard value. Lastly, topographic wetness index (TWI), an indicator of the influence of local topography on water movement and accumulation, was calculated using the equation:

$$TWI = \ln(\alpha/\tan\beta) \qquad (1)$$

where α is the upslope contributing area calculated using a D-infinity algorithm (Tarboton 1997) and β is the slope angle (Beven and Kirkby 1979).

Estimating Automatic Growing Season Efflux

To sum continuous F_S across time, we gap-filled our observations using a regression model from Sullivan and others (2010) based upon modeled soil temperature and water content:

$$\ln(F_S) = \beta_0 + \beta_1 T + \beta_2\theta + \beta_3\theta^2 \qquad (2)$$

where F_S is soil CO_2 efflux (μmol m^{-2} s^{-1}), β_n is a parameter coefficient, T is soil temperature at 5 cm, and θ is volumetric soil water content at 5 cm (m^3 m^{-3}). We attempted to fit simpler equations, but we determined Eq. (2) was the preferred method to gap-fill based on Akaike's Information Criterion (Akaike 1974), adjusted R-squared, root mean square error, and mean absolute error. Final model performances found all variables to be significant (p-value < 0.001); and across all chambers and years, the fraction of F_S from gap-filling averaged 29.0% in the growing season and 30.4% in total (Supplemental Table 2). Gap-filled data are displayed in Figure 2. Once the dataset was gap-filled, we calculated growing season fluxes from automatic chambers by summing all hourly fluxes between May 9 and Oct 15 of each year (Table 1), as well as annual fluxes summed for the calendar year (Supplemental Table 3). We also simulated annual estimates from manual sampling for 2016–2018 by randomly choosing one observation from the automatic gap-filled dataset each week between 0900 and 1200 h in hours without rain, linearly interpolating between daily observations, and summing for the calendar year (Supplemental Figure 1).

We focused our statistical analyses on growing season estimates to align automatic measurements with manual measurements. Further, we ensured that our analyses were robust to gap-filling methods by calculating growing season F_S using three additional methods (Supplemental Figure 1) from the R package "FluxGapsR" (version 0.1.0) (Zhao and others 2020). One method, singular spectrum analysis, is independent of soil moisture and temperature (Zhao and others 2020), which ensures F_S estimates are not an artifact of the Flux-PIHM model.

Data Analysis

We first assessed the impact of topographic positions, climatic variability, and sampling methods on growing season F_S through total least squares (TLS) regression and repeated measures analysis of variance (ANOVA). We regressed manual and automatic growing season F_S from all gap-filling methods using TLS regression, which accounts for variability within both estimates. Further, we explored the impact of landscape position and sampling method across 2016 and 2017 growing season F_S using a three-way repeated measures ANOVA. Significant interaction effects were explored separately for manual methods and automatic methods in post-hoc two-way and one-way repeated measures ANOVAs.

However, these statistical approaches have weaknesses that we overcame using a Random Forest (RF) model to explore controls on daily F_S predictions. RF is a supervised machine learning algorithm used for classification and regression (Breiman 2001). A detailed description is available in Hoffman and others (2018). Briefly, RF is built upon the concept of recursive partitioning, a non-parametric method that creates decision trees by recursively splitting response variables at a series of nodes into clusters of similar observations. This method is ideal for both our time series and geospatial data, because it is relatively free of assumptions regarding the distribution of variables and regarding the relationships between predictor and response variables. However, individual decision trees are sensitive to the training data and prone to overfitting. RF offers more robust predictions by constructing many independent regression trees and generating the mean prediction across all trees. An ensemble of trees is grown using bootstrapped samples of observations split at a user-defined number of randomly chosen predictor variables. From this ensemble, RF algorithms provide several useful outputs, two of which we display: variable importance score, which ranks predictor variables based on the contribution of each variable to overall model accuracy, and partial dependence plots, which explore the relationship between one predictor (or two interacting predictors) and the response averaged across all observations (Strobl and others 2007).

We built the RF model using the R package "randomForest" (version 4.7–1.1) (Breiman and Cutler 2018). We trained the RF model to predict observed daily F_S using days without any gap-filled hours ($n = 3966$) using 16 predictor variables: mean daily soil water content ($m^3\ m^{-3}$); mean daily soil temperature (°C); cumulative 3-week precipitation (mm); mean daily air temperature (°C); planform curvature; profile curvature; standard curvature; elevation (m); total soil depth (m); topographic wetness index; 90th percentile daily green chromatic coordinate; percent soil carbon in the O Horizon, 0–5 cm, and 5–15 cm; and percent clay at 0–5 cm and 5–15 cm. Hourly values were aggregated to mean daily values for soil moisture and soil temperature, because green chromatic coordinate data were not reliable at all hourly timesteps (for example, photographs cannot be collected at night). Precipitation and air temperature were aggregated to the timestep with the largest Spearman rank correlation coefficient (Benjamini-Hoberg-adjusted p-value < 0.001) (Spearman 1904; Benjamini and Hochberg 1995). We optimized the number of trees (n_{tree}) and the number of predictor variables considered at each node for splitting (m_{try}), such that $n_{tree} = 1000$ and $m_{try} = 5$. After optimization, the RF model was retrained on two subsets of the data: swales and valley floors, which we call convergent ($n = 1851$), and planar midslopes and ridgetops, which we call non-convergent ($n = 2115$). These datasets were randomly split into 70% for model training and 30% for model validation. We repeated this split 10 times to estimate the uncertainty of variable importance scores from subsampling the training data (as in Saha and others 2021). We assessed model performance through percent variance explained and ordinary least squares linear regression between observed and predicted daily F_S for the validation dataset. All statistical analyses were performed in R (version 4.1) software (R Core Team 2018), and code for the Random Forest model is available via GitHub (https://github.com/MWKopp/Ecosystems2022).

Results

Growing Season Soil CO_2 Efflux from Continuous Measurements

Our first hypothesis was that adding terrain variables to standard soil temperature and moisture predictors would explain significantly more variance in estimates of growing season and daily F_S across climate variability. We first tested this hypothesis through repeated measures ANOVA of growing season F_S from continuous measurements across landscape positions (Supplemental Table 4). Growing season F_S from automatic chambers ranged from 610 ± 63 to 1350 ± 139 g C m^{-2} 180 day^{-1} across all topography and years (Table 1).

However, measurements within a landscape position varied widely—and, for ridgetop and valley floors, significantly—across years. Two-way repeated measures ANOVA found support for a significant effect of year on growing season F_S (F value = 14.539, p value = 0.009) and a significant interaction effect between year and landscape position (F value = 8.643, p value = 0.012). These significant effects seem to be driven by two trends: (1) F_S from ridgetop and valley floors show a bidirectional response to interannual climate variability, and (2) F_S from non-convergent flow paths varied more across years. Specifically, growing season F_S from ridgetops increased by 463 g C m^{-2} 180 day^{-1} between average estimates from the driest year (2016) to wettest year (2018), while valley floors decreased by an average of 208 g C m^{-2} 180 day^{-1} (Table 1). Though this response is less clear for midslopes, planar midslopes (non-convergent) also showed the highest growing season F_S in the wettest year, with an increase of 424 g C m^{-2} 180 day^{-1} relative to the driest year (Table 1). Convergent flow paths varied widely within years (evidenced by relatively high standard errors in Table 1), which may have masked responses across years for swale midslopes. In short, data from automatic chambers support capturing topography as a significant interactive predictor of interannual growing season F_S in the Shale Hills catchment.

Random Forest Modeling of Daily Soil CO_2 Efflux

Our next test of the first hypothesis was to explore the predictive power of topographic, soil, and climate variables in modeling daily F_S from automatic chambers using a Random Forest (RF) approach. We trained a RF model to predict daily F_S using 16 variables from days without any missing (that is, gap-filled) hours of automatic data. Using all data, the overall final RF model explained 77.8% ($\pm$ 0.02) of the variation in the data using 13 variables. Topographic wetness index (TWI), standard curvature, and green chromatic coordinate (GCC) were removed from the final model, because other variables accounted for these mechanisms. For example, standard curvature is a combination of planform and profile curvature, and GCC was highly correlated with air temperature. To compare predictors of F_S and their interactions across topography, we retrained this model on two subsets of the overall data: convergent (swales and valleys) and non-convergent areas (planar midslopes and ridgetops). These models explained 76.92% ($\pm$ 0.03) of the variation in data from convergent areas and 79.87% ($\pm$ 0.02) of the variation from non-convergent areas.

We compared predictions from the final RF models with observations in our validation dataset to assess model performance. Pearson correlations between predicted and observed daily F_S showed strong positive correlation from convergent (r = 0.82, p value < 0.001) and non-convergent areas (r = 0.89, p value < 0.001). Ordinary least squares linear regression between observations and predictions yielded an average slope of 1.00 ($\pm$ 0.00) and 1.02 ($\pm$ 0.02) for convergent and non-convergent areas, respectively. As such, we consider model performance to be robust.

To understand the variables driving RF model predictions, we calculated variable importance scores and partial dependence plots. Variable importance scores are a metric that ranks predictors based on the relative contribution of each variable to overall model accuracy. For convergent flow areas, the most important variables influencing F_S were 5-cm soil temperature and mean daily air temperature, which showed a median percent increase in mean square errors across models of 71.07 $\pm$ 0.10 and 54.26 $\pm$ 0.10, respectively (Figure 3). For non-convergent areas, the most important variable was also soil temperature (68.89 $\pm$ 0.15); however, this was closely followed by 3-week antecedent precipitation (64.29 $\pm$ 0.19) and 5-cm volumetric soil water content (64.15 $\pm$ 0.22). Whereas variable importance scores explore the relationship between all predictors, partial dependence plots explore the relationship between one predictor (here, soil moisture) or the interaction of two predictors (here, soil moisture and temperature) and the response averaged across all observations. For non-convergent areas, soil moisture and daily F_S displayed a monotonically increasing relationship with a greater amplitude of change in F_S (Figure 4a). For convergent areas, soil moisture and daily F_S displayed a parabolic relationship (Figure 4b). These relationships remain even when accounting for the interactive effects of soil temperature (Figure 4c and Figure 4d). Overall, RF models suggest that accounting for convergent flow may change the relative importance of and relationship between dominant predictors and daily F_S.

Comparing Growing Seasons Estimates Across Automatic and Manual Methods

Our second hypothesis was that automated chamber methods will provide the same F_S estimates as

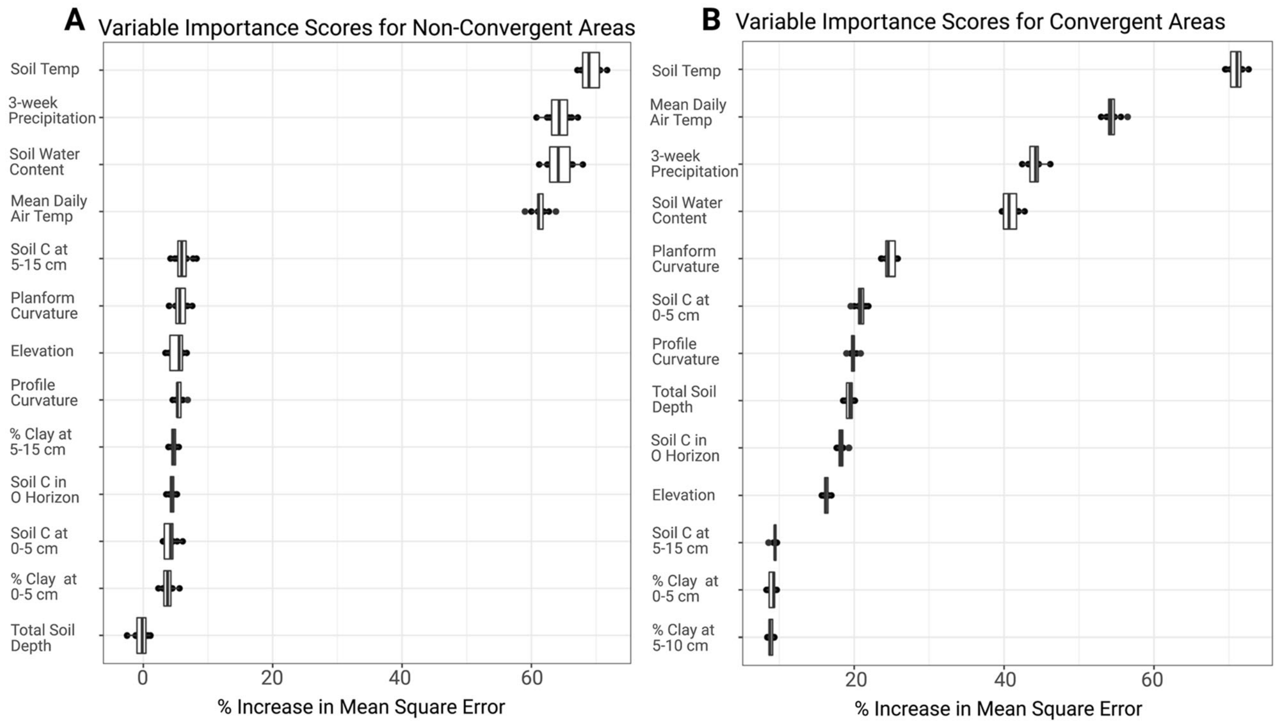

Figure 3. Variable importance scores from Random Forest models for daily soil CO_2 efflux (F_S) predictions trained on only observed data from (A) non-convergent areas (ridgetops and planar midslopes) and (B) convergent areas (swales and valley floors). Variables are ranked by relative importance for predicting F_S, where a greater percent increase in mean square error indicates greater importance in the model. Ten variable importance scores were calculated by a Random Forest model built on ten separate random subsamples of training data. These ten variable importance scores are represented as a box plot corresponding to each variable to estimate uncertainty. Random Forest models were trained on observation only (that is, not gap-filled) data from automated flux chambers.

manual sampling when aggregated to the growing season temporal scale and catchment spatial scale. However, three-way repeated measures ANOVA (Supplemental Table 4) found a significant effect of method (F value = 7.280, p value = 0.021) on growing season F_S estimates, as well as a significant interaction effect between year (2016–2017) and method (F value = 7.866, p value = 0.019).

To test the magnitude of the method effect, and its interaction with year, we compared growing season F_S estimates from both methods using total least squares linear regression. We found growing season F_S estimates from automatic methods to be 1.25 ($\pm$ 0.08) times greater than manual estimates across all landscape positions and both years (Figure 5). This effect tended to be greater in a dry year (1.45 $\pm$ 0.06) than an average year (1.11 $\pm$ 0.06) and greater in convergent (1.27 $\pm$ 0.11) than non-convergent (1.21 $\pm$ 0.10) areas (Supplemental Table 5).

We ensured that this difference was not an artifact of gap-filling automatic estimates by repeating regressions with three other gap-filling methods, both across and within years; regardless of treatment of automatic data, estimates from automatic chambers were consistently greater than from manual methods (regression slope with a 95% confidence interval $>$ 1 in Supplemental Table 5). Although manual data were only collected in 2016 and 2017, simulating annual F_S estimates for manual methods by randomly drawing from the automated chamber dataset across 2016–2018 also found consistently lower estimates than automatic methods (Supplemental Figure 1).

Discussion

We present one of the first multi-year continuous soil CO_2 efflux (F_S) datasets to capture the interactions of both complex terrain and significant precipitation variability in a temperate deciduous forest. Leveraging this dataset, we found a bidirectional response of F_S across the catchment to increasing interannual water availability. We discuss the mechanisms driving this response as well as their implications for predicting and monitoring F_S in complex terrain.

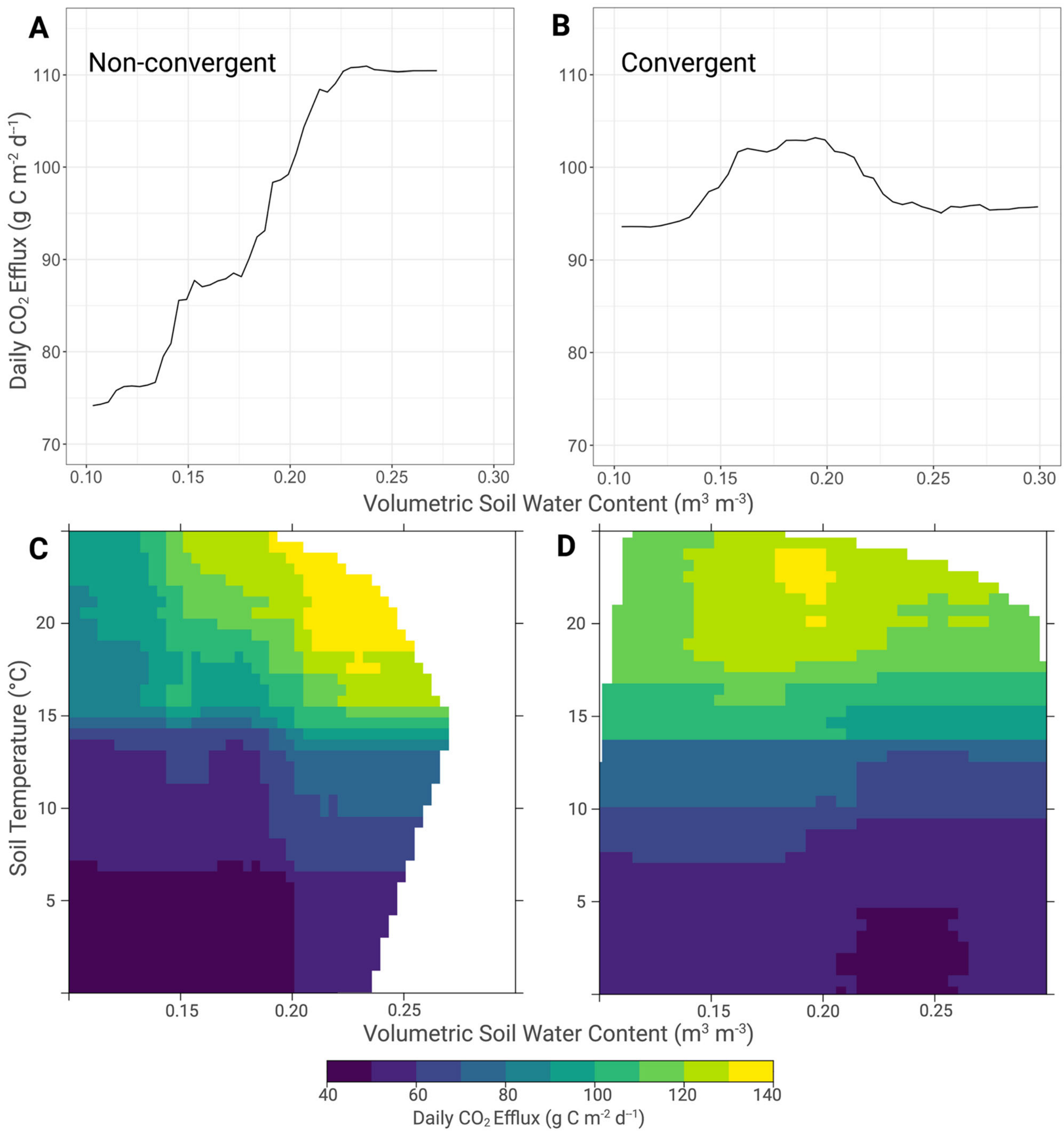

Figure 4. Partial dependence plots of dominant predictors on daily F_S from Random Forest models. Partial dependence plots show the average relationship between modeled 5-cm soil moisture and daily F_S across **a** non-convergent areas (ridgetops and planar midslopes) and **b** convergent areas (swales and valley floors). Multipredictor partial dependence plots show the average interactive effect of modeled 5-cm soil moisture and temperature on daily F_S across **c** non-convergent areas and **d** convergent areas. White areas in multipredictor plots are regions outside of the observed range used to train the Random Forest model. Random Forest models were trained on observation only (that is, not gap-filled) data.

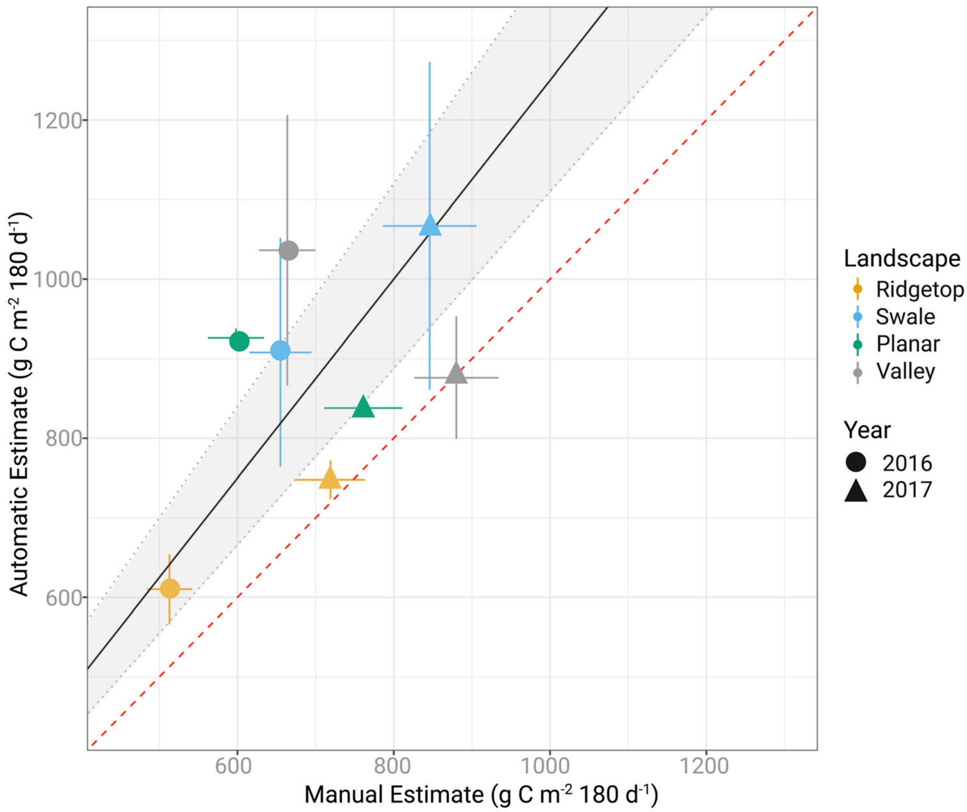

Figure 5. Regression between estimated growing season F_S (g C m^{-2} 180 days^{-1}) from manual and automatic chamber methods. The red dashed line indicates a theoretical 1:1 line. The black line indicates the total least squares linear regression between methods (slope = 1.25) with a 95% confidence interval shaded in gray. Regression coefficients are similar regardless of gap-filling methods for automatic methods (see Supplemental Table 5). Vertical standard error lines are greater (that is, more variability along the y axis), because automatic chambers have fewer replicates (n = 2) relative to manual sampling (n = 7 to 21, depending on landscape position).

Using Automated Chambers to Estimate F_S Responses Across Topography and Climate

The significance of complex terrain for C storage and fluxes has generated a pressing need to understand and predict the response of F_S to climate variability across topographic gradients (for example, Rotach and others 2014; Senar and others 2018). Yet maximizing spatial coverage in monitoring F_S has relied on manual sampling methods (for example, Riveros-Iregui and others 2012; Savage and Davidson 2001), which limit sampling frequencies to coarse timescales (for example, Hanson and others 1993) that may miss significant short-term (sub-daily) responses to climatic disturbances. Automatic chambers offer an opportunity to monitor F_S at a fine temporal resolution; however, their cost limits spatial replication. With a sampling design that explicitly accounts for terrain, we find that hillslope position is a significant control on interannual F_S (Supplemental Table 4) beyond what can be captured by instantaneous soil moisture and temperature.

A key finding is that terrain position determines the direction of response to traditionally measured soil and climatic predictors of F_S. Specifically, growing season F_S from ridgetops at Shale Hills increased with increasing interannual water availability, while valley floors showed decreasing annual F_S in increasingly wet years (Table 1). These results not only corroborate previous research that interannual precipitation variability leads to a bidirectional response of F_S in complex terrain (Riveros-Iregui and others 2012; Berryman and others 2015), but expand this exploration from drought/non-drought comparisons in semiarid and (sub)alpine forests to record annual precipitation in a humid temperate forest. While we found a considerable range in both hourly F_S (0.00 g C m^{-2} h^{-1} to 1.78 g C m^{-2} h^{-1}) and growing season F_S (610 $\pm$ 63 to 1350 $\pm$ 139 g C m^{-2} 180 day^{-1}), this range is comparable to other F_S observations in temperate forests (Giasson and others 2013). Moreover, these estimates are comparable to observations from forests in complex terrain (Berryman and others 2015; Riveros-Iregui and McGlynn 2009) and modeled estimates for our study site (Shi and others 2018). In short, continuously monitoring a few key positions in complex terrain identified a bidirectional response of F_S to interannual climate variability within comparable ranges to manual monitoring across an order of magnitude more spatial replicates (for example, Riveros-Iregui and others 2009; Primka 2021).

Untangling Mechanisms of the Bidirectional Response: Moisture-Versus Diffusion-Limited $\boldsymbol{F}_S$

Our work advances F_S research by showing that monitoring soil moisture and temperature variation is not enough to estimate and predict F_S—landscape context is critical for knowing how soil moisture affects F_S. We hypothesize that the bidirectional response of F_S to interannual water availability hinges on the spatial distribution of mechanisms dominantly limiting F_S: diffusion limitations in areas receiving convergent flows, and water limitations to biological activity in non-convergent areas.

In convergent areas, such as swales and valley floors, F_S responds based on a parabolic relationship with soil water content (Riveros-Iregui and others 2012). Generally, F_S peaks at intermediate soil moisture conditions (Doran and others 1991), which we confirm for our site in Random Forest models (Figure 4b, d). In topographic positions with wetter soils, such as the deep, clay-rich valley floors at Shale Hills (Lin and others 2006), persistent high soil moisture reduces diffusivity, and oxygen availability limits aerobic respiration (Hodges and others 2019). However, these wet sites could dry under reduced hydrologic connectivity, such as during a summer drought, which could promote a large release of CO_2 from enhanced microbial and root respiration (Davidson and others 1998; Senar and others 2018). This is one likely explanation for the flush of F_S from the valley floor in 2016. Under the dry conditions of 2016, valley floor soils may have dried enough to increase oxygen diffusion into the soil surface, increasing aerobic respiration. A concurrent study at Shale Hills measured soil pO_2 at nearby valley floor position and found a marked increase in $\%O_2$ at all soil depths in the drought summer of 2016 relative to the summer of 2017 (Hodges and others 2019). This increase in soil pO_2 may have allowed for the breakdown of available C substrates. Alternatively, increased diffusivity in 2016 may have allowed accumulated soil pCO_2 to move from soil storage into the atmosphere (Hassenmueller and others 2015). In contrast, increased precipitation in 2018 may have led to soils that were too wet for maximum F_S. Under saturated conditions, there is limited diffusion of pO_2 for aerobic respiration; and, even when microbial communities switch to anaerobic respiration (evidenced by redox features in Lin and others 2006, and direct measurements of pCO_2/pO_2 in Hodges and others 2019), limited diffusion leads to a build-up of pCO_2 rather than a flush of F_S (Hassenmueller and others 2015). This may explain the decrease in F_S from convergent areas at high volumetric soil water content (Figure 4b). In short, shifts in biological activity and diffusivity may explain interannual F_S variability in valley floor positions at Shale Hills, leading to large fluxes in drought years and lower fluxes in wet years.

By contrast, interannual variability in F_S from non-convergent areas, such as ridgetops and planar midslopes, may reflect water limitation to biological activity rather than limitation by low O_2 or slow CO_2 diffusion. Whereas convergent areas display a parabolic relationship with soil moisture, daily F_S from non-convergent areas monotonically increased with increasing soil moisture (Figure 4a). Ridgetops at Shale Hills have thinner, sandier soils that drain quickly (Lin and others 2006). In a dry year, water in soil pores may be disconnected, limiting dissolved organic carbon (DOC) supply for microbial activity and lowering heterotrophic respiration (Papendick and Campbell 1981). Similarly, drought stress on trees could limit photosynthesis or C allocation to new or maintained root growth, lowering autotrophic respiration (Bryla and others 1997; Wang and others 2014). Supporting this hypothesis, minirhizotron data from the same spatially distributed sites in this study showed decreased root tip production in drier years relative to wetter years in 2016–2018 (Primka IV and others 2022). In a wet year, water in soil pores is connected, which allows water and DOC to reach microbial communities, increasing heterotrophic respiration. Additionally, tree roots may also access shallow water near the soil surface, upon which most trees at Shale Hills depend for water uptake (Gaines and others 2015), such that growth and maintenance root respiration are not water limited. Together, these sources contribute to an increase in F_S in wet years such that ridgetop F_S equals or exceeds F_S from valley floors (Table 1; Supplemental Table 3), despite valley floor soils having greater C storage (Andrews and others 2011) and soil pCO_2 (Hassenmueller and others 2015; Hodges and others 2019). Overall, contrasting limiting factors on F_S across convergent and non-convergent areas lead to opposing responses of F_S across interannual climatic variability.

Implications for Predictions: Random Forest Models Unveil Topography-Mediated Interactions with Soil Moisture

Random Forest (RF) models are among the machine learning tools rapidly improving predictions of soil greenhouse gas emissions (for example, Saha and others 2021). For example, Lu and others (2021) found RF models outperformed ten common process-based terrestrial ecosystem models for global F_S predictions. As such, coupling automatic chamber data with RF models offers one of the best methods to model complex interactions among drivers of F_S at fine temporal scales (Lu and others 2021). Our RF models found soil temperature, soil moisture, and climate variables were dominant predictors of F_S, but their relative importance (Figure 3) and relationship with daily F_S (Figure 4) differed between areas receiving convergent flow or not.

We expected that soil temperature would have great predictive power, because soil temperature is the most common predictor used to model F_S (for example, Arrhenius 1889; van't Hoff 1898; Lloyd and Taylor 1994). While soil temperature did have high importance values in RF models across the landscape, soil moisture and 3-week antecedent precipitation were nearly as important for predicting daily F_S from non-convergent areas (Figure 3). Other topographic (elevation and curvature) and soil (texture, C, and total depth) characteristics had low importance values in non-convergent areas (Figure 3a). By contrast, daily F_S from convergent areas had higher importance values for soil and air temperature, with moderate predictive power from moisture variables (soil and 3-week precipitation) and some predictive power from curvature, surface and O horizon soil C, and total soil depth (Figure 3b). If further studies find that these results hold true in other ecosystems, then simple and remotely sensed terrain metrics may improve which predictors we choose to scale F_S from small but topographically complex catchments to larger scale models.

Relative to soil temperature, the relationship between F_S and soil moisture varies widely across studies, which has hampered the development of empirical equations translating soil moisture parameters into reliable F_S predictions (Lou and others 2006). Generally, optimum F_S is predicted to occur at intermediate soil moisture, whether in statistical correlations (for example, Doran and others 1991) or more complex mechanistic models (for example, Davidson and others 2011). Beneath some soil moisture threshold, F_S is most limited by slow diffusion of soluble C substrates into extracellular enzymes and by microbes involved in decomposition (Papendick and Campbell 1981), which can lead to dormancy in microbes and diminish heterotrophic respiration (Fierer and Schimel 2002). Similarly, drought conditions can decrease photosynthesis, which decreases translocation of photosynthates to the rhizosphere for root respiration (Ruehr and others 2009). Under these dry soil conditions, F_S has a positive—sometimes even linear (Jassal and others 2008)—relationship with soil water availability yet has little response to soil temperature (Suseela and others 2012).

However, we suggest that some non-convergent areas may never reach or remain at volumetric soil water contents above this intermediate optimum long enough to decrease F_S, leading to a relationship which appears monotonically increasing rather than parabolic (Figure 4a), even when accounting for interactive effects with soil temperature (Figure 4c). Despite training RF models with data from 2018, the wettest year on record in the state of our study site, F_S from non-convergent areas does not display the decrease expected by limited diffusion of soluble-C and O_2. Overall, the flush of F_S from water-limited non-convergent soils in a wet year may suggest a shift in the topographic positions dominantly contributing to catchment-level F_S at Shale Hills as the climate transitions toward wetter conditions (Ning and others 2012).

Implications for Methods: Targeting Control Points of Between-Method Variability

A current hypothesis in F_S research is that manual and automatic chamber methods, although imbued with different biases (Yao and others 2009), balance a spatial and temporal tradeoff that produce similar estimates, particularly when scaling up across time (Savage and Davidson 2003). While both methods capture interannual variability in growing season F_S across the Shale Hills watershed, the choice of method significantly affected the magnitude of estimates (Supplemental Table 4). Estimates from automatic chambers averaged 1.25 ± 0.08 times greater than from manual methods (Figure 5). Underpinning this variability is an interactive effect between methods, climate, and landscape positions. We find the difference between methods was most pronounced in a dry year (2016) and in areas receiving convergent flow (swales and valley floors) (Supplemental Table 5). Specifically, we find estimates from automatic chambers in a dry year to be 1.45 ± 0.06 greater than from manual estimates across the catchment, which is significantly more than in an average year (1.11 ± 0.06). These findings caution that the assumption of consistent F_S estimates across sampling methods may hold true under average climatic conditions in well-drained landscapes but may be violated in areas receiving convergent flow.

There are several explanations for differences between methods at this site. First, automatic chambers may be biased by aspect. Shale Hills is a V-shaped catchment with a north- and south-facing slope. Although manual methods captured variability across aspect, automatic chambers were located on the south-facing slope, which may have greater F_S from relatively greater SOC storage (Andrews and others 2011) and more solar radiation leading to warmer soils. As such, automatic chambers may overrepresent, and thus overestimate, the ''hot spots'' in the catchment. However, a more likely explanation is that manual methods may be biased by an underestimation of diurnal variation. A growing body of research finds that accounting for nighttime fluxes leads to higher F_S estimates from automatic chambers, whether from lags in response to physical and biological changes (Makita and others 2018; Phillips and others 2011) or from measurement bias (Brændholt and others 2017). At Shale Hills, there is preliminary evidence of pronounced diurnal variation (Kopp, unpublished data), which automatic chambers more accurately capture (Yao and others 2009). This explanation is further supported by our simulated manual sampling, which found notably lower annual F_S estimates from all automatic chambers when excluding nighttime observations (Supplemental Figure 1). These findings support previous suggestions that the fine temporal resolution of automatic chambers combined with the spatial distribution of manual methods complement landscape-scale monitoring of greenhouse gas emissions (Savage and others 2014). In complex terrain, we further refine this suggestion to strategically place automatic chambers at ecosystem control points (Bernhardt and others 2017) disproportionately responsive to climatic variability, such as valley floors (activated in dry years) and ridgetops (activated in wet years).

Though such ecosystem control points may be relatively rare on the landscape, their pronounced variability for between-method variation has implications for scaling F_S across space. To consider these implications, we performed a simple spatial scaling exercise to estimate average catchment-scale growing season F_S. We weighted the average growing season F_S from convergent or non-convergent flow paths by their relative area within Shale Hills (that is, 22% of total catchment area is convergent, while 78% is non-convergent, as in Smith and others 2017). In 2016 (a dry year), we estimate average catchment-scale growing season F_S to be 813 and 578 g C m^{-2} 180 day^{-1} from automatic and manual methods, respectively. In 2017 (an average year), we estimate average catchment-scale F_S to be 824 and 760 g C m^{-2} 180 day^{-1} from automatic and manual methods, respectively. These estimates are consistent with our within-year regressions between methods and emphasize that the choice of method could lead to similar catchment-scale estimates in an average growing season or to about 28.9% error when failing to capture ''hot moments,'' such as from convergent areas in a dry year or at night. This error may be substantial even when hot moments are relegated to patches representative of a small fraction of the total catchment area. In short, F_S monitoring designs in complex terrain may need to account for significant interactive effects between methods and landscape positions, particularly as interannual climatic conditions become increasingly variable.

Conclusions

We use one of the first multi-year F_S sampling schemes that captures both fine spatial and temporal heterogeneity to demonstrate that hillslope position and shape can explain variance of daily, seasonal, and interannual F_S estimates from a temperate deciduous forest in complex terrain. By capturing fine spatial heterogeneity, we find that landscape context is critical for understanding how F_S (bidirectionally) responds to soil moisture. We hypothesize this response hinges on the spatial distribution of limiting factors on F_S—slow diffusion limits F_S from areas receiving convergent flows, and water availability for biota limits F_S from non-convergent areas. Although soil saturation limitations on F_S are well known in wetland and laboratory soil incubations, our work contributes to an understanding of when and where this process occurs in upland soils and the factors that govern its spatial distributions. Even in upland soils, our results show that accounting for convergent flow paths can change the relative importance and relationship of predictors of daily F_S. Further, by capturing fine temporal heterogeneity, we find that the choice of sampling frequency has a significant effect on growing season F_S estimates.

Moreover, our findings could have implications for scaling F_S to global predictions in Earth System Models (ESM) by demonstrating how sub-grid topographic heterogeneity can lead to significant spatiotemporal variability of F_S within less than 1–km^2. In a review of 16 ESMs, Todd-Brown and others (2013) found that most ESMs could not reproduced grid-scale spatial heterogeneity of soil C or its decomposition. The authors posited that this poor performance was due, in part, to inadequate representations of topographic and soil moisture interactions, with some models assuming all soil C decomposition has a monotonically increasing relationship with soil moisture regardless of landscape position (Todd-Brown and others 2013). Our research suggests that sub-grid F_S may display a parabolic relationship with soil moisture depending on lateral redistribution of water, yet this redistribution is rarely included in ESM land models (Clark and others 2015). Clark and others (2015) recommend using ESMs that capture sub-grid soil moisture heterogeneity, such as the Catchment model (Koster and others 2000) or the tiled hydrology implementation of the LM3 model (Subin and others 2014), to resolve uncertainties in land–atmosphere fluxes. We further suggest that, if our results hold true elsewhere, ESMs could incorporate simple and remotely sensed terrain metrics to partition the parabolic relationship between sub-grid soil moisture and F_S into the full range (that is, decreasing F_S at high soil moisture for convergent areas) or a range drier than the inflection point (that is, monotonically increasing F_S for non-convergent areas). Future work should test how this approach might improve current uncertainty in spatial patterns of soil C and its decomposition across global ecosystems.

ACKNOWLEDGEMENTS

This manuscript was improved by feedback from Drs. Elise Pendall, Ben Bond-Lamberty, and three anonymous peer reviewers. Financial support was provided by National Science Foundation Grant (award EAR—1331726) for the Susquehanna Shale Hills Critical Zone Observatory (SSHCZO), by the US Department of Energy, Office of Science, Office of Biological & Environmental Research (award DE—SC0012003), and by Hatch Appropriations under Project PEN04571 and Accession 1003346. Manual soil CO_2 efflux samples were collected by Alexandra Buck and Jeremy Harper. All data were collected from the SSHCZO field site, which is managed by Brandon Forsythe, within Penn State's Stone Valley Forest, which is managed by staff of the Forestlands Management Office and funded by the Penn State College of Agricultural Sciences and Department of Ecosystem Science and Management. PhenoCam data are funded by the Northeastern States Research Cooperative, NSF's Macrosystems Biology program (Awards EF–1065029 and EF–1702697), and DOE's Regional and Global Climate Modeling program (Award DE–SC0016011). MK was funded by a USDA National Needs Fellowship from NIFA (Grant 2019–38420–28979) and trained on an NSF Research Traineeship (NSF-DGE NRT-INFEWS # 1828822).

REFERENCES

Akaike H. 1974. A new look at the statistical model identification. IEEE Transactions on Automatic Control 19:716–723.

Andrews DM, Lin H, Zhu Q, Jin L, Brantley SL. 2011. Hot Spots and Hot Moments of Dissolved Organic Carbon Export and Soil Organic Carbon Storage in the Shale Hills Critical Zone Observatory. Vadose Zone Journal 10:943–954.

Arrhenius, S. 1889. On the Reaction Velocity of the Inversion of Cane Sugar by Acids. Zeitschrift für physikalische Chemie 4: 226ff.

Benjamini Y, Hochberg Y. 1995. Controlling the False Discovery Rate: A Practical and Powerful Approach to Multiple Testing. Journal of the Royal Statistical Society: Series b. 57:289–300.

Bernhardt ES, Blaszczak JR, Ficken CD, Fork ML, Kaiser KE, Seybold EC. 2017. Control Points in Ecosystems: Moving Beyond the Hot Spot Hot Moment Concept. Ecosystems 20:665–682.

Berryman EM, Barnard HR, Adams HR, Burns MA, Gallo E, Brooks PD. 2015. Complex terrain alters temperature and moisture limitations of forest soil respiration across a semiarid to subalpine gradient. Journal of Geophysical Research Biogeoscience 120.

Beven KJ, Kirkby MJ. 1979. A physically based, variable contributing area model of basin hydrology. Hydrological Sciences Journal 24:43–69.

Bond-Lamberty B, Thomson A. 2010. Temperature-associated increases in the global soil respiration record. Nature 464:7288.

Bond-Lamberty B, Christianson DS, Malhotra A, Pennington SC, Sihi D, AghaKouchak A, et al. 2020. COSORE: A community database for continuous soil respiration and other soil-atmosphere greenhouse gas flux data. Global Change Biology 26:7268–7283.

Brændholt A, Larsen KS, Ibrom A, Pilegaard K. 2017. Overestimation of closed-chamber soil CO_2 efflux at low atmospheric turbulence. Biogeosciences 14:1603–1616.

Brantley S, White T, West N, Williams J, Forsythe B, Shapich D, … Gu X. 2018. Susquehanna Shale Hills Critical Zone

Observatory: Shale Hills in the Context of Shaver's Creek Watershed. Vadose Zone Journal 17.

Breiman L. 2001. Random Forests. Machine Learning 45:5–32.

Breiman L, Cutler A. 2018. Breiman and Cutler's Random Forests for Classification and Regression. Retrieved from https://cran.r-project.org/web/packages/randomForest/randomForest.pdf

Bryla DR, Bouma TJ, Eissenstat DM. 1997. Root respiration in citrus acclimates to temperature and slows during drought. Plant Cell and Environment 20:1411–1420.

Clark MP, Fan Y, Lawrence DM, Adam JC, Bolster D, Gochis DJ, Hooper RP, Kumar M, Leung LR, Mackay DS, Maxwell RM, Shen C, Sweson SC, Zeng X. 2015. Improving the representation of hydrologic processes in Earth System Models. Water Resources Research 51:5929–5956.

Courtois EA, Stahl C, Burban B, Van den Berge J, Berveiller D, Bréchet L, Soong JL, Arriga N, Peñuelas J, Janssens IA. 2019. Automatic high-frequency measurements of full soil greenhouse gas fluxes in a tropical forest. Biogeosciences 16:785–796.

Dai Y, Dickinson RE, Wang Y. 2004. A Two-Big-Leaf Model for Canopy Temperature, Photosynthesis, and Stomatal Conductance. Journal of Climate 17:2281–2299.

Davidson EA, Belk E, Boone RD. 1998. Soil water content and temperature as independent or confounded factors controlling soil respiration in a temperate mixed hardwood forest. Global Change Biology 4:217–227.

Davidson EA, Samanta S, Caramori SS, Savage K. 2011. Dual Arrhenius and Michaelis-Menten kinetics model for decomposition of organic matter at hourly to seasonal time scales. Global Change Biology 18(1):371–384.

Doran JW, Mielke IN, Power JF. 1991. Microbial activity as regulated by soil water-filled pore space. In: Ecology of Soil Microorganisms in the Microhabital Environments (pp 94–99). Transactions of the 14th Int. Congress of Soil Sci. Symposium.

Eissenstat D, Wubbles J, Adams T, Osborne J. 2013. Susquehanna Shale Hills Critical Zone Observatory Tree Survey (2008). Integrated Earth Data Applications (IEDA). https://doi.org/10.1594/IEDA/100268.

Fierer N, Schimel JP. 2002. Effects of drying–rewetting frequency on soil carbon and nitrogen transformations. Soil Biology & Biogeochemistry 34:777–787.

Friedlingstein P, Meinshausen M, Arora V, Jones C, Anav A, Liddicoat S, Knutti R. 2014. Uncertainties in CMIP5 Climate Projections due to Carbon Cycle Feedbacks. Journal of Climate 27.

Friedlingstein P, O'Sullivan M, Jones MW, Andrew RM, Hauck J, Olsen A, et al. 2020. Global Carbon Budget 2020. Earth Syst. Sci. Data 12:3269–3340.

Gaines KP, Stanley JW, Meinzer FC, McCulloh KA, Woodruff DR, Adams TS, Lin H, Eissenstat DM. 2015. Reliance on shallow soil water in a mixed-hardwood forest in central Pennsylvania. Tree Physiology 36:444–458.

Giasson MA, Ellison AM, Bowden RD, Crill PM, Davidson EA, Drake JE, Frey SD, Hadley JL, Lavine M, Melillo JM, Munger JW, Nadelhoffer KJ, Nicoll L, Ollinger SV, Savage KE, Steudler PA, Tang J, Varner RK, Wofsy SC, Foster DR, Finzi AC. 2013. Soil respiration in a northeastern US temperate forest: a 22-year synthesis. Ecosphere 4:140.

Görres CM, Kammann C, Ceulemans R. 2016. Automation of soil flux chamber measurements: potentials and pitfalls. Biogeosciences 13:1949–1966.

Guo Q. 2019. SSHCZO Digital Elevation Model (DEM), GIS/Map Data, Land Cover, LiDAR, Soil Survey—Shale Hills (2010). HydroShare. https://www.hydroshare.org/resource/cea8dda7b8c64f76aaaf412d8d37f041/#citation

Hanson PJ, Wullschleger SD, Bohlman SA, Todd DE. 1993. Seasonal and topographic patterns of forest floor CO_2 efflux from an upland oak forest. Tree Physiology 13:1–15.

Hasenmueller EA, Jin L, Stinchcomb GE, Lin H, Brantley SL, Kaye JP. 2015. Topographic controls on the depth distribution of soil CO2 in a temperate watershed. Applied Geochemistry 63:58–69.

Hashimoto S, Carvalhais N, Ito A, Migliavacca M, Nishina K, Reichstein M. 2015. Global spatiotemporal distribution of soil respiration modeled using a global database. Biogeosciences 12(13):4121–4132.

He Y. 2019. Understanding the Carbon Cycle in Complex Terrain at the Shale Hills Critical Zone Observatory. [Dissertation.] The Pennsylvania State University.

Hodges C, Kim H, Brantley SL, Kaye JP. 2019. Soil CO2 and O2 Concentrations Illuminate the Relative Importance of Weathering and Respiration to Seasonal Soil Gas Fluctuation. Soil Science Society of America Journal 83:1167–1180.

Hoffman AL, Kemanian AR, Forest CE. 2018. Analysis of climate signals in the crop yield record of sub-Saharan Africa. Global Change Biology 24:143–157.

Hufkens K. 2021. 'daymeter.' https://cran.r-project.org/web/packages/daymetr/index.html.

Jassal RS, Black AT, Novak MD, Gaumont-Guay D, Nesic Z. Effect of soil water stress on soil respiration and its temperature sensitivity in an 18-year-old temperate Douglas-fir stand. Global Change Biology 14: 1305–1318.

Jian J, Vargas R, Anderson-Teixeira KJ, Stell E, Herrmann V, Horn M, Kholod N, Manzon J, Marchesi R, Paredes D, Bond-Lamberty BP. 2021. A Global Data of Soil Respiration Data, Version 5.0. ORNL DAAC, Oak Ridge, Tennessee, USA.

Jiang Y, Zhang B, Wang W, Li B, Wu Z, Chu C. 2020. Topography and plant community structure contribute to spatial heterogeneity of soil respiration in a subtropical forest. Science of the Total Environment 733.

Kettler TA, Doran JW, Gilbert TL. 2001. Simplified Method for Soil Particle-Size Determination to Accompany Soil-Quality Analyses. Soil Science Society of America Journal 65:849–852.

Koster RD, Suarez MJ, Ducharne A, Stieglitz M, Kumar P. 2000. A catchment-based approach to modeling land surface processes in a general circulation model: 1. Model structure. Journal of Geophysical Research 105:809–824.

Le Quéré C, Andrew RM, Canadell JG, Sitch S, Ivar Korsbakken J, Peters GP, et al. 2016. Global Carbon Budget 2016. Earth System Science Data 8:2.

Lin HS, Kogelmann W, Walker C, Bruns MA. 2006. Soil moisture patterns in a forested catchment: A hydropedological perspective. Geoderma 131:345–368.

Lin H. 2019. SSHCZO—Ground Penetrating Radar (GPR), Geology, GIS/Map Data—GPR Bedrock Elevation GIS Data—Shale Hills (2008). HydroShare. https://www.hydroshare.org/resource/ee157df1b4c84799a2d2c748d3a0b679/#citation.

Liu Q, Edwards NT, Post WM, Gu L, Ledford J, Lenhart S. 2006. Temperature-independent diel variation in soil respiration observed from a temperate deciduous forest. Global Change Biology 12:2136–2145.

Lloyd J, Taylor JA. 1994. On the Temperature Dependence of Soil Respiration. Functional Ecology 8:315–323.

Lou Y, Zhou X, editors. 2006. Soil Respiration and the Environment. Elsevier.

Lovett GM, Turner MG, Jones CG, Weathers KC, editors. 2005. Ecosystem Function in Heterogeneous Landscapes. Springer.

Lu H, Li S, Ma M, Bastrikov V, Chen X, Ciais P, Dai Y, Ito A, Ju W, Lienert S, Lombardozzi D, Lu X, Maignan F, Nakhavali M, Quine T, Schindlbacher A, Wang J, Wang Y, Wårlind D, Zhang S, Yuan W. 2021. Comparing machine learning-derived global estimates of soil respiration and its components with those from terrestrial ecosystem models. Environmental Research Letters 16:054048.

Makita N, Kosugi Y, Sakabe A, Kanazawa A, Ohkubo S, Tani M. 2018. Seasonal and diurnal patterns of soil respiration in an evergreen coniferous forest: Evidence from six years of observation with automatic chambers. Plosone 13:e0192622.

Mao J, Ricciuto DM, Thornton PE, Warren JM, King AW, Shi X, Iversen CM, Norby RJ. 2016. Evaluating the Community Land Model in a Pine Stand with Shading Manipulations and $^{13}CO_2$ Labeling. Biogeosciences 13:641–657.

Nelson DW, Sommers LE. 1996. Total Carbon, Organic Carbon, and Organic Matter. Sparks DL, ed. Methods of Soil Analysis, Part 3. Chemical Methods. Madison, WI: American Society of Agronomy. p961–1010.

Ning L, Mann ME, Crane R, Wagener T, Najjar RG, Singh R. 2012. Probabilistic Projections of Anthropogenic Climate Change Impacts on Precipitation for the Mid-Atlantic Region of the United States. Journal of Climate 25:5273–5291.

NOAA. 2007. US divisional and station climatic data and normal. Natl. Clim. Data Ctr., Asheville, NC.

NOAA. 2021. Climate at a Glance: Statewide Time Series. www.ncdc.noaa.gov/cag/statewide/time-series/36/pcp/ann/1/1895-2021?base_prd=true&begbaseyear=1901&endbaseyear=2000.

Orr, AS. 2016. Topographic controls on root partitioning patterns in a temperate forest. [Master's thesis]. The Pennsylvania State University.

Pacific VJ, McGlynn BL, Riveros-Iregui DA, Welsh DL, Epstein HE. 2008. Variability in Soil Respiration across Riparian-Hillslope Transitions. Biogeochemistry 91:51–70.

Pacific VJ, McGlynn BL, Riveros-Iregui DA, Welsch DL, Epstein HE. 2011. Landscape structure, groundwater dynamics, and soil water content influence soil respiration across riparian–hillslope transitions in the Tenderfoot Creek Experimental Forest, Montana. Hydrological Processes 25:811–827.

Papendick RI, Campbell GS. 1981. Theory and Measurement of Water Potential. In: Water Potential Relations in Soil Microbiology. Soil Science Society of America Special Publications Number 9 (eds Parr JF, Gardner WR, Elliot LF), 1–22. Soil Science Society of America, Inc., Madison, WI.

Petrakis S, Seyfferth A, Kan J, Inamdar S, Vargas R. 2017. Influence of experimental extreme water pulses on greenhouse gas emissions from soils. Biogeochemistry 133:147–164.

Phillips CL, Nickerson N, Risk D, Bond BJ. 2011. Interpreting diel hysteresis between soil respiration and temperature. Global Change Biology 17:515–527.

Primka EJ, IV. 2021. Fine root dynamics and their effect on soil CO_2 efflux across a forested landscape with complex topography. [Dissertation]. The Pennsylvania State University.

Primka EJ IV, Adams TS, Buck A, Eissenstat DM. 2021. Topographical shifts in fine root lifespan in a mixed, mesic temperate forest. PLoS ONE 16(7):e0254672.

Primka EJ, IV, Adams TS, Buck A, Eissenstat DM. 2022. Shifts in root dynamics along a hillslope in a mixed, mesic temperate forest. Plant and Soil: 1–17.

R Core Team. 2018. R: A language and environment for statistical computing. R Foundation for Statistical Computing, Vienna, Austria. https://www.R-project.org/.

Reyes WM, Epstein HE, Li X, McGlynn BL, Riveros-Iregui DA, Emanuel RE. 2017. Complex terrain influences ecosystem carbon responses to temperature and precipitation. Global Biogeochemical Cycles 31.

Richardson AD, Hufkens K, Milliman T, Aurecht DM, Chen M, Gray JM, Johnston MR, Keenan TF, Klosterman ST, Kosmala M, Melaas EK, Friedl MA, Frolkin S. 2018. Tracking vegetation phenology across diverse North American biomes using PhenoCam imagery. Nature 5:180028.

Riveros-Iregui DA, McGlynn BL, Epstein HE, Welsch DL. 2008. Interpretation and evaluation of combined measurement techniques for soil CO_2 efflux: Discrete surface chambers and continuous soil CO_2 probes. Journal of Geophysical Research 113:1–11.

Riveros-Iregui DA, McGlynn BL. 2009. Landscape structure control on soil CO_2 efflux variability in complex terrain: Scaling from point observations to watershed scale fluxes. Journal of Geophysical Research 114.

Riveros-Iregui DA, McGlynn BL, Emanual RE, Epstein HE. 2012. Complex terrain leads to bidirectional responses of soil respiration to inter-annual water availability. Global Change Biology 18:749–756.

Rubio VE, Detto M. 2017. Spatiotemporal variability of soil respiration in a seasonal tropical forest. Ecology and Evolution 7:7104–7116.

Ruehr NK, Offermann CA, Gessler A, Winkler JB, Ferrio JP, Buchmann N, Barnard RL. 2009. Drought effects on allocation of recent carbon: From beech leaves to soil CO2 efflux. New Phytology 184(4):950–961.

Ruehr NK, Knohl A, Buchmann N. 2010. Environmental variables controlling soil respiration on diurnal, seasonal and annual time-scales in a mixed mountain forest in Switzerland. Biogeochemistry 98:153–170.

Rotach MW, Wohlfahart G, Hansel A, Reif M, Wagner J, Gohm A. 2014. The World is Not Flat: Implications for the Global Carbon Balance. American Meteorological Society.

Saha D, Basso B, Robertson GP. 2021. Machine learning improves predictions of agricultural nitrous oxide (N2O) emissions from intensively managed cropping systems. Environmental Research Letters 16.

Savagae KE, Davidson EA. 2001. Interannual variation of soil respiration in two New England forests. Global Biogeochemical Cycles 0: 1–14.

Savage KE, Davidson EA. 2003. A comparison of manual and automated systems for soil CO2 flux measurements. Journal of Experimental Botany 54:891–899.

Savage KE, Phillips RL, Davidson EA. 2014. High temporal frequency measurements of greenhouse gas emissions from soils. Biogeosciences 11:2709–2720.

Schlesinger WH, Bernhardt E. 2013. Biogeochemistry, An Analysis of Global Change. Waltham, MA: Elsevier.

Senar OE, Webster KL, Creed IF. 2018. Catchment-Scale Shifts in the Magnitude and Partitioning of Carbon Export in Response to Changing Hydrologic Connectivity in a Northern Hardwood Forest. JGR Biogeosciences 123:2337–2352.

Shi Y, Baldwin DC, Davis KJ, Yu X, Duffy CJ, Lin H. 2015. Simulating high-resolution soil moisture patterns in the Shale Hills watershed using a land surface hydrologic model. Hydrological Processes 29:4624–4637.

Shi Y, Davis KJ, Duffy CJ, Yu X. 2013. Development of a coupled land surface hydrologic model and evaluation at a critical zone observatory. Journal of Hydrometeorology 14:1401–1420.

Shi Y, Eissenstat DM, He Y, Davis KJ. 2018. Using a spatially-distributed hydrologic biogeochemistry model with a nitrogen transport module to study the spatial variation of carbon processes in a Critical Zone Observatory. Ecological Modelling 380:8–21.

Smeglin YH, Davis KJ, Shi Y, Eissenstat DM, Kaye JP, Kaye MW. 2020. Observing and Simulating Spatial Variations of Forest Carbon Stocks in Complex Terrain. Journal of Geophysical Research: Biogeosciences 125.

Smith L, Eissenstat DM, Kaye MW. 2017. Variability in aboveground carbon dynamics driven by slope aspect and curvature in an eastern deciduous forest, USA. Canadian Journal of Forest Research 47:149–158.

Spearman C. 1904. The proof and measurement of association between two things. American Journal of Psychology. 15:72–101.

Strobl C, Boulesteix AL, Zeileis A, Horthorn T. 2007. Bias in Random Forest variable importance measures: Illustrations, sources and a solution. BMC Bioinformatics 8.

Subin Z, Milly P, Sulman B, Malyshev S, Shevliakova E. 2014. Resolving terrestrial ecosystem processes along a subgrid topographic gradient for an earth-system model. Hydrology and Earth System Sciences 11:8443–8492.

Sullivan BW, Dore S, Kolb TE, Hart SC, Montes-Helu MC. 2010. Evaluation of methods for estimating soil carbon dioxide efflux across a gradient of forest disturbance. Global Change Biology.

Suseela V, Conant RT, Wallenstein MD, Dukes JS. 2012. Effects of soil moisture on the temperature sensitivity of heterotrophic respiration vary seasonally in an old-field climate change experiment. Global Change Biology 18:336–348.

Tian Q, Wang D, Tang Y, Li Y, Wang M, Liao C, Liu F. 2019. Topographic controls on the variability of soil respiration in a humid subtropical forest. Biogeochemistry 145:177–192.

Tarboton DG. 1997. A new method for the determination of flow directions and contributing areas in grid digital elevation models. Water Resour. Res. 33:309–319.

Thornton MM, Wei Y, Thornton PE, Shrestha R, Kao S, Wilson BE. 2020. Daymet: Station-Level Inputs and Cross-Validation Result for North America, Version 4. ORNL DAAC, Oak Ridge, Tennessee, USA.

Throop HL, Archer SR, Monger HC, Waltman S. 2012. When bulk density methods matter: Implications for estimating soil organic carbon pools in rocky soils. Journal of Arid Environments 77:66–71.

Todd-Brown KEO, Randerson JT, Post WM, Hoffman FM, Tarnocai C, Schuur EAG, Allison SD. 2013. Causes of variation in soil carbon simulations from CMIP5 Earth system models and comparison with observations. Biogeosciences 10.

van'T Hoff, JH. 1898. Sur la loi de dilution des sels. Recl. Trav. Chim. Pays-Bas Belg. 17:370–372.

Wang Y, Hao Y, Cui XY, Zhao H, Xu C, Zhou X, Xu Z. 2014. Responses of soil respiration and its components to drought stress. Journals of Soils and Sediments 14:99–109.

Wang C, Lai X, Zhu Q, Castellano MJ, Yang G. 2019. Soil Type, Topography, and Land Use Interact to Control the Response of Soil Respiration to Climate Variation. Forests 10.

Xiao D, Li L. 2018. Shale Hills CZO Hourly Precipitation Total Data. Retrieved from http://www.czo.psu.edu/data_precipho ur-sh2.html.

Xia Y, Mitchell K, Ek M, Sheffield J, Cosgrove B, Wood E, Luo L, Alonge C, Wei H, Meng J, Livneh B, Lettenmaier D, Koren V, Duan Q, Mo K, Fan Y, Mocko D. 2012. Continental-scale water and energy flux analysis and validation for the North American Land Data Assimilation System project phase 2 (NLDAS-2): 1. Intercomparison and application of model products. J. Geophys. Res. 117: D03109.

Yan T, Song H, Wang Z, Teramoto M, Wang J, Liang N, Ma Z, Sun Z, Zi Y, Li L, Peng S. Temperature sensitivity of soil respiration across multiple time scales in a temperate plantation forest. Science of the Total Environment 668: 479–485.

Yao ZS, Zheng XH, Xie BH, Liu CY, Mei BL, Dong HB, Butterbach-Bahl K, Zhu JG. 2009. Comparison of manual and automated chambers for field measurements of N2O, Ch4, CO2 fluxes from cultivated land. Atmospheric Environment 43:1888–1896.

Zhao J, Lange H, Meissner H. 2020. Gap-filling continuously-measured soil respiration data: A highlight of time-series-based methods. Agricultural and Forest Meteorology 285.